Optical and dielectric properties of isothermally crystallized nano $KNbO_3$ in Er^{3+}-doped K_2O-Nb_2O_5-SiO_2 glasses

Reenamoni Saikia Chaliha[a], K. Annapurna[a], Anal Tarafder[a], V. S. Tiwari[b], P. K. Gupta[b] and Basudeb Karmakar[a,*]

[a]*Glass Technology Laboratory, Glass Division, Central Glass and Ceramic Research Institute (Council of Scientific and Industrial Research), 196, Raja S.C. Mullick Road, Kolkata 700032, India*
[b]*Laser Materials Development and Devices Division, Raja Ramanna Center for Advanced Technology, Indore 452 013, India*

_____

Abstract

Precursor glass of composition $25K_2O$-$25Nb_2O_5$-$50SiO_2$ (mol %) doped with Er_2O_3 (0.5 wt % in excess) was isothermally crystallized at 800^oC for 0-100 h to obtain transparent $KNbO_3$ nanostructured glass-ceramics. XRD, FESEM, TEM, FTIRRS, dielectric constant, refractive index, absorption and fluorescence measurements were carried out to analyze the morphology, dielectric, structure and optical properties of the glass-ceramics. The crystallite size of $KNbO_3$ estimated from XRD and TEM is found to vary in the range 7-23 nm. A steep rise in the dielectric constant of glass-ceramics with heat-treatment time reveals the formation of ferroelectric nano-crystalline $KNbO_3$ phase. The measured visible photoluminescence spectra have exhibited green emission transitions of $^2H_{11/2}$, $^4S_{3/2} \rightarrow {}^4I_{15/2}$ upon excitation at 377 nm ($^4I_{15/2} \rightarrow {}^4G_{11/2}$) absorption band of Er^{3+} ions. The near infrared (NIR) emission transition $^4I_{13/2} \rightarrow {}^4I_{15/2}$ is detected around 1550 nm on excitation at 980 nm ($^4I_{15/2} \rightarrow {}^4I_{11/2}$) of absorption bands of Er^{3+} ions. It is observed that photoluminescent intensity at 526 nm ($^2H_{11/2} \rightarrow {}^4I_{15/2}$), 550 nm ($^4S_{3/2} \rightarrow {}^4I_{15/2}$) and 1550 nm ($^4I_{13/2} \rightarrow {}^4I_{15/2}$) initially decrease and then gradually increase with increase in heat-treatment time. The measured lifetime (τ_f) of the $^4I_{13/2} \rightarrow {}^4I_{15/2}$ transition

also possesses a similar trend. The measured absorption and fluorescence spectra reveal that the Er^{3+} ions gradually enter into the $KNbO_3$ nanocrystals.

Keywords: Transparent glass-ceramic; Nano-crystallized Er^{3+}: $KNbO_3$; Luminescence; Ferroelectric crystals; Dielectric constant.

[*]Corresponding author. Tel.: +91-33 2473 3469; fax: +91-33 2473 0957

E-mail address: basudebk@cgcri.res.in (B. Karmakar)

1. Introduction

Ferroelectric potassium niobate (KNbO$_3$, KN) has the A^{1+}B^{5+}O$_3$ perovskite-type (orthorhombic) crystal structure (crystal symmetry class *mm2*; unit cell dimensions: a = 5.6896 Å, b = 3.9693 Å and c = 5.7256 Å) and having large nonlinear coefficient (d$_{33}$ = 27.4 pm/V at 1064 nm). It is widely used in frequency doubling, tunable wave guiding, active laser host, holographic storage and surface acoustic wave [1-3]. Consequently, it becomes a subject of intense study. Very recently, potassium niobate ceramics were revisited in the interest of a search for environmental friendly lead-free piezoelectric and nonlinear materials [4]. Due to the low cost and high speed fabrication process of glass technology in comparison to single crystal preparation, with the flexibility of tailored properties to produce transparent nanostructures by controlled crystallization, ferroelectric KNbO$_3$ containing transparent glass-ceramics have generated increasing academic and technological interests. A large electro-optic effect (r$_{42}$ = 380 pm/V for KNbO$_3$ [3]) has been observed in a number of transparent glass-ceramic materials containing a ferroelectric crystalline phase. Several isothermal or non-isothermal studies have been carried out with a view to generate KNbO$_3$, KNbSi$_2$O$_7$, K$_3$Nb$_3$Si$_2$O$_{13}$ etc. ferroelectric crystal phases in various compositions of the K$_2$O-Nb$_2$O$_5$-SiO$_2$ (KNS) glass system [5-10] and noticed strong second harmonic generation (SHG). It is observed that these glass-ceramics doped with rare earth (RE) ions, become very good luminescent media which are able to generate and amplify light. This application in combination with inherent nonlinear optical (NLO) properties of ferroelectric crystals, could offer a possibility to design self frequency doubling laser sources [3]. Hence, it is considered more interesting and important to explore crystallization of RE (here, Er^{3+}) doped

ferroelectric crystal (here, $KNbO_3$) producing glasses. To the best of our knowledge, there is no previous report on nanostructured crystallization of erbium (III), Er^{3+} ion doped $K_2O-Nb_2O_5-SiO_2$ glasses.

In comparison to the other rare earth ions, Er^{3+} has been extensively used as the most suitable active ion in several hosts by normal fluorescence for optical amplification at 1.5 µm. Trivalent erbium ions characterized by the $^4I_{13/2} \rightarrow {}^4I_{15/2}$ intra-4f transition play the key role in near infrared (NIR) emission [11]. Besides, Er^{3+} doped glasses are chosen for getting better lasing property that can act as an eye-safe laser sources near 1550 nm. The photoluminescent emission intensity of erbium doped glasses is mainly dependent on the chemical environment of Er^{3+} ion because in the excited state Er^{3+} ion can de-excite by either photon emission at 1.53 µm, or non-radiative relaxation through coupling to a quenching site. Also, if the symmetry of the local crystal field around the erbium ion in the host glass is not distorted, the emission of erbium ion is forbidden. Therefore, the erbium ions must be incorporated in a non-centrosymmetric host material for strong optical emission [12, 13]. Similarly, under favorable conditions strong green emission at 551 nm is possible upon normal high energy excitation.

The dielectric property of amorphous solids is different from that of crystalline solids. Due to the high spontaneous polarization (P_s = 0.41 C/m^2 for $KNbO_3$) as well as induced polarization of ferroelectric crystals under applied electric field, the difference in the dielectric properties (ε =137 for $KNbO_3$ [14]) is remarkably large than that of the glass [3]. Therefore, it is important to study the dielectric properties (dielectric constant) with progress of crystallization of precursor glasses of ferroelectric crystals.

In view of the significant and potential advantages as stated above, here we focus our systematic analysis on structural, optical and dielectric properties of isothermally nanostructured crystallization of $KNbO_3$ in Er^{3+}-doped $25K_2O$-$25Nb_2O_5$-$50SiO_2$ (mol %) glasses. The crystallization process has been studied by differential thermal analysis (DTA), X-ray diffraction (XRD), refractive index, dielectric constant, field emission scanning electron (FESEM) and transmission electron microscopy (TEM) and Fourier transform infrared reflection spectroscopy (FTIRRS) analyses as well.

2. Experimental

The glass of the chemical composition of $25K_2O$-$25Nb_2O_5$-$50SiO_2$ (mol %) doped with 0.5 wt % Er_2O_3 (in excess) was prepared using high purity K_2CO_3 (GR, 99%, Alfa Aesar), Nb_2O_5 (GR, 99.5%, Alfa Aesar), SiO_2 (99.99%) and Er_2O_3 (99.99%, Alfa Aesar) by melting the well mixed chemical batch of 100 g glass in a platinum crucible at 1550^oC for 2 h. The melt was homogenized with two intermittent stirrings and later it was quenched by pouring onto a pre-heated iron mould. In order to remove the internal stresses the glass block was subsequently annealed at 600^oC for 1 h. The as-prepared glass block was cut into desired dimensions and polished for undertaking different measurements.

The density of the as-prepared glass was measured by following the standard Archimedes' principle using distilled water as the buoyancy liquid. The DTA curve of powdered glass was recorded on a Netzsch STA 409 C/CD instrument from room temperature to 900^oC at a heating rate of 10^oC/min. The polished samples were heat-treated at 800^oC for 1, 2, 3, 5, 10, 25, 50 and 100 h after nucleating at 720^oC temperature

for 2 h. The refractive indices of glass and heat-treated samples at five different wavelengths (473, 532, 632.8, 1064 and 1552 nm) were measured by a prism coupling measurement technique (Model Metricon 2010/M).

The XRD pattern was recorded using an Xpert-Pro diffractometer (CuKα) with nickel filtered and anchor scan parameters wavelength of 1.54060 Å at 25^oC having the source power of 40 kV and 30 mA to identify the possible phases. The nanocrystallinity of the heat-treated glasses was examined by both FESEM and TEM. A Carl Zeiss high resolution field emission electron microscope (FESEM) (model SUPRA 35 VP) with the parameters gun vacuum = 3×10^{-10} mbar, system vacuum = 2.65×10^{-5} mbar and extractor current = 159.3 μA for FESEM measurement. Freshly fractured surfaces of the heat-treated glasses were etched in 1% HF solution for 150 s and were coated with a thin carbon film for the above measurements. And the TEM was done on FEI (Tecnai G^2) instrument. The dielectric constant of all samples was measured at room temperature using a Hioki LCR meter (Model: 3532-50 LCR Hitester) at 1 MHz frequency.

The fluorescence emission and excitation spectra of the Er^{3+} doped as-prepared and heat-treated samples were measured on an enhanced performance NIR continuous bench top modular spectrofluorometer from Photon Technology International (Model: QuantaMaster) attached with Hamamatsu NIR-PMT (P1.7R) as detector and Xe arc lamp as excitation source. The lifetime was measured with the same instrument using a 75W Xe flash lamp.

3. Results and discussion

3.1 Physical, optical and thermal properties

The prepared glass was transparent with body color of pink. From the measured glass density, refractive indices (n_e, $n_{F'}$ and $n_{C'}$) at three different wavelengths and other related optical properties have been determined using relevant expressions, and the results are presented in Table 1. From Table 1 it is clear that the refractive index and density of potassium niobium silicate glass are higher than those of normal soda lime silicate glasses. The large refractive indices of these glasses are due to the presence of highly polarizable Nb^{5+} ions with high ionic refraction, 24.5 [15]. It is observed that ions with an empty or unfilled d-orbital such as Nb^{5+} ion (outer electronic configuration: $4d^05s^0$) contributes very strongly to the linear and nonlinear polarizabilities [16]. For the same reason, this glass is also possessing a high value of molar refractivity ($R_M = 14.95$ cm^3) and electronic polarizability ($\alpha = 5.592 \times 10^{-24}\,cm^3$) [17, 18].

The DTA curve was recorded for the precursor glass powder and is shown in Fig. 1. It exhibits an inflection in the temperature range 647-689°C followed by an exothermic peak at 759°C (T_p) corresponding to the phase crystallization. The point of intersection of the tangents drawn at the slope change as marked in Fig. 1 of the DTA curve estimates the glass transition temperature (T_g). These are listed in Table 1. From the DTA data, the glass thermal stability factor ($\Delta = T_p - T_g$) has been determined and found to be 78°C. Reasonably, high glass stability factor specifies the ability of this glass in forming nano-structured glass-ceramic under controlled heat-treatment. The exothermal peak at 759°C in the DTA thermogram can be attributed to the growth of $KNbO_3$ crystallites from nuclei in the glass bulk. The heat-treated glass-ceramics were also transparent as the precursor

glass. The transparencies of the precursor glass and resultant nano glass-ceramics are shown in Fig. 2 as they are laid down on writing. The refractive indices of glass and heat-treated samples at five different wavelengths (473, 532, 632.8, 1064 and 1552 nm) are shown in Fig. 3. It is seen that the refractive indices of heat-treated samples of 2 and 50 h increases rapidly as compared to precursor glass. These are due to the formation of $KNbO_3$ crystals having high refractive index (2.2912 at 600 nm [19]).

3.2 XRD analysis

Fig. 4(a) shows the X-ray diffractograms of as-prepared glass along with the glass-ceramic samples. The amorphous nature of the as-prepared glass is indicated by the XRD pattern consisting of only a broad and halo band at around 29° diffraction angle. The structuring of this halo band takes place in the XRD pattern of the heat-treated glass-ceramic samples of 1-100 h along with the appearance of other well defined peaks around 25°, 28.5^o, 30°, 32.8^o and 51.5^o diffraction angles, which confirms the precipitation crystalline phase in the amorphous matrix. The crystalline phase resembles the JCPDS cards 32-821 and 32-822 of known potassium niobate. Using the following Scherrer's formula, the average crystallite sizes (diameter, d) were calculated from the full width at half maximum (FWHM) values of the diffraction peaks detectable in the traces of 1-100 h in Fig. 4(a) [20].

$$d = 0.9\lambda/\beta \cos\theta \qquad (1)$$

where λ is the wavelength of X-ray radiation (CuKα = 1.5406Å), β is the FWHM of the peak at 2θ. The diffraction peak located around 2θ = 30° has been considered for this estimation. The calculated average crystallite sizes lie in the range 7-15 nm. The gradual

increase of crystallite size as a function of heat-treatment duration is presented in Fig. 4(b).

3.3 FESEM and TEM images analyses

The morphology and crystallite size in glass-ceramic samples have been examined by FESEM and TEM images analyses. The FESEM photomicrographs of the sample heat-treated at 800°C for 3 and 50 h duration are presented in Figs. 5(a) and 5(b) respectively. From the FESEM micrographs, it is clearly observed that the glassy matrix of the heat-treated samples initially phase separated on nanometric scale followed by incipient precipitation of defined crystallites within the Nb-K rich phase regions on prolonged heat-treatments. The droplets have irregular shape spreading out uniformly through out the bulk glass matrix and the size of which can be estimated to be 47-66 nm. The TEM and high resolution TEM (HRTEM) images of the sample heat treated for 50 h have also been presented in Figs. 5(c) and 5(d) respectively. The inset in Fig. 5(c) represents its selected area electron diffraction (SAED) pattern. From the SAED, the measured Miller indices are 220 resembling the potassium niobate crystal in the JCPDS card file no. 9-156. The atomic or lattice fringes of formed crystallites have been clearly observed in HRTEM image and the distance between any two planes is found to be 9.4 Å. The formed lattice planes from the HRTEM image resemble well with the d-spacing of the planes as reported in the JCPDS card file no. 49-824 of known potassium niobate. Another interesting result is arising out of the comparison of the FESEM and TEM micrographs with the XRD data. The crystallites size are 7-15 and 14-23 nm as estimated from the XRD patterns and TEM image respectively. The particle size calculated from

TEM is to some extent higher than those from XRD. This is due to the fact that XRD analysis gives the average sizes of the entire (very small to big) crystallites whereas TEM photograph exhibits the crystallites of some specific places. For this reason, the latter is smaller than the former. However, these sizes are smaller than the single droplet size of 47-66 nm as observed in FESEM, which suggests that the crystallization starts at the interface between the droplets and the matrix. The growth of the crystallites takes place inside these droplets, so the droplets are polycrystalline. This phenomenon causes a change of the matrix composition, which prevents the further growth of the crystallites, regardless of the increase in the heat-treatment time, and a stable transparent biphasic structure by a change of the density of inhomogeneities in the matrix is formed [9, 21-22].

3.4 Fourier transform infrared reflectance spectroscopy

Fig. 6 shows the comparative FTIR reflectance spectra (FTIRRS) of the precursor glass and samples heat-treated at 800ºC for 2 and 100 h duration in the wavenumber range 500-2000 cm^{-1}. Its inset shows the reflectivity at 930 and 749 cm^{-1} of precursor glass and heat-treated glasses as a function of heat-treatment time. It is seen that the FTIRR spectrum of the precursor glass exhibits a broad reflection band centered at 930 cm^{-1} as a result of wider distribution of SiO_4 structural units. This is an indication of the structural disorder exists in the amorphous network with the presence of SiO_4 tetrahedra and NbO_6 octahedra with different number of non-bridging oxygens, and attributed to overlapping of Si-O and Nb-O stretching vibrations. In spite of the transparent nature of the heat-treated samples, the FTIR reflectance spectra of 2 and 100

h reveal narrowing of the main reflection band with additional features arising at 1128, 749 and 598 cm^{-1} in comparison to the as-prepared glass [6].

Considering the stronger force constant of the Si-O bonds than that of Nb-O ones, the reflection bands can be assigned in the FTIR reflectance spectra [23]. In the FTIRR spectra, the stretching modes of the Si-O-Si bonds of the SiO$_4$ tetrahedra with nonbridging oxygen (NBO) atoms are active in 900-1000 cm^{-1} range and the stretching modes of the Nb-O bonds in the NbO$_6$ octahedra occur in the 700-800 cm^{-1} range [24].

It is seen that there are structural modifications occurring in the glass matrix as a result of the heat-treatment as revealed by the variation of the FTIRR spectra of the as-prepared glass from that of the heat-treated glasses. The rearrangement of the glassy matrix is an indicative of the fact that the alkali enriched phase begins to crystallize producing a nanostructure with the heat-treatment. The reflection bands around 1050 - 1150 cm^{-1} are associated with the ν_3 antisymmetric stretching vibration modes of the SiO$_4$ tetrahedra. The symmetric stretching mode ν_1 is assigned to the reflection bands lying in the range 800-1000 cm^{-1} wavenumber. The reflection band at 1128 cm^{-1} and 930 cm^{-1} wavenumber can be related to the asymmetric and symmetric stretching vibration modes of Si-O bonds in SiO$_4$ tetrahedra respectively, while the band at 749 cm^{-1} is due to the Nb-O stretching modes of distorted NbO$_6$ octahedra [25, 26]. Hence, it is revealed that in a phase separated matrix of the heat-treated samples, the crystallization starts at the interface between the two phases originating a redistribution of both types of structural units such as NbO$_6$ octahedra and SiO$_4$ tetrahedra. This corroborates that the reflection band centered at 749 cm^{-1} wavenumber is assigned to the KNbO$_3$ crystal formation. Very slow increase in the intensity of this reflection band with the increase in

heat-treatment time indicates that the further growth of $KNbO_3$ nanocrystallites at the interface is prevented for longer heat-treatment times to satisfy the chemical composition required by the crystallizing phase [23] but the reflectivity of the 100 h heat-treated sample is more intense than sample heat-treated for 2 h. This is also confirmed by the relative intensity ratio (I_{Nb-O}/I_{Si-O}) of the reflection bands at 749 cm^{-1} to 930 cm^{-1} as given Table 2. Further, FTIRR spectra of all the samples as shown in Fig. 6 exhibit a band around 598 cm^{-1}. It is assigned as ν_2 bending vibrational modes of the Si-O bonds in the SiO_4 tetrahedra. Thus from the investigations carried out on the measured FTIR reflectance spectra of Er^{3+} doped potassium niobium silicate glass and glass-ceramics as described above provide the information of crystallization with initial phase separation followed by advancement of $KNbO_3$ crystal formation in the glass matrix. The results of the FTIRRS are in good agreement with that of XRD, FESEM and TEM studies.

3.5 Dielectric constant

As prepared Er^{3+} doped potassium niobium silicate glass has exhibited relatively higher value of dielectric constant ($\varepsilon =17$) than the normal glasses sodalime silicate ($\varepsilon =7$-10) [8-10] or borosilicate glasses ($\varepsilon =4.5$-8) [6-8] due to high ionic refraction of Nb^{5+} ion ($R_i = 24.5$) as described earlier. Fig. 7 shows the magnitude of dielectric constant increase steeply (from $\varepsilon =17$ to $\varepsilon =31$)) in the case of the heat-treated samples and thereafter it maintains almost saturation for any further heat treatment time. This suggests that on heat-treatment, at the initial stages, separation of silica rich phase and K–Nb enriched phases takes place and with the further prolonged heat-treatments incipient precipitation of $KNbO_3$ having high dielectric constant ($\varepsilon =137$) [14] and spontaneous polarization, P_s

= 0.41 C/m^2 [3]. The variation in crystallite size distributions and also the distribution of the $KNbO_3$ phase in the microstructure are the causes for the differences in the dielectric constant values amongst the heat-treated samples [5]. This result is again in conformity with the conclusions made from XRD, FESEM and TEM measurements on the nano-crystallization of $KNbO_3$ phase in the glass matrix.

3.6 Optical absorption spectra

Fig. 8 shows the representative UV-Vis-NIR absorption spectra of Er^{3+} doped as-prepared glass and heat-treated samples for 2, 50 and 100 h duration. The absorption occurs due to the *4f-4f* electric dipole transitions from the ground $^4I_{15/2}$ state to different excited state of Er^{3+} ions. The absorption spectra have very strong absorption edges below 350 nm and exhibit ten numbers of distinct absorption peaks which are similar to those appeared in silicate, tellurite and chloro sulphide glasses [27-32]. All the peaks were assigned in accordance with Carnall's convention as $^4I_{15/2} \rightarrow {}^2G_{9/2}$ (365 nm), $^4G_{11/2}$ (377 nm), $^2H_{9/2}$ (406 nm), $^4F_{5/2} + {}^4F_{3/2}$ (450 nm), $^4F_{7/2}$ (488 nm), $^2H_{11/2}$ (521 nm), $^4S_{3/2}$ (544 nm), $^4F_{9/2}$ (651 nm), $^4I_{9/2}$ (799 nm) and $^4I_{11/2}$ (978 nm) [33]. From this figure it is noticed that the base lines of the absorption spectra of heat-treated samples have been elevated significantly with diminishing intensities of the absorption peaks. Also the FWHM values of the peaks for the transitions $^4I_{15/2} \rightarrow {}^4G_{11/2}$ and $^4I_{15/2} \rightarrow {}^2H_{11/2}$ are 4.28 and 6.69 nm for precursor glass whereas 3.56 and 6.42 nm respectively for heat-treated samples. All these phenomena confirm that the laser active Er^{3+} ions have entered into the $KNbO_3$ crystalline phase. Similar facts have also been observed in our earlier work on Eu^{3+} doped $KNbO_3$ glass-ceramics [34].

The uplifting of the base line for glass-ceramic sample due to scattering imparted by the nanocrystallite phase is discussed as follows. Normally the decrease of optical transmission of the glass-ceramics happens mainly because of two reasons, one is the crystallite size and the other is the refractive index difference between crystalline and residual amorphous phase. In this system, the crystallite size is found to be in nanometric (7-15 nm) scale which smaller than the visible wavelength. But the refractive index of the formed $KNbO_3$ phase is found to be considerably higher (RI = 2.2912 at 600 nm [19]) than the residual glassy phase (RI = 1.7681 at 632.8 nm, see Fig. 3); hence the later case may be responsible for changes observed in the measured optical absorption spectra. This is in accordance to the Rayleigh scattering model since the crystallites (7-15 nm) are smaller than $\lambda/20$ for visible wavelengths. The scattering loss τ, is given by [35]

$$\tau = 32\pi^4 d^3 (n\Delta n)^2 NV/3\lambda^4 \qquad (2)$$

where d is the particle diameter, λ the wavelength of light, n the refractive index, N the number density of particles, and V the volume of the particle. From the absorption spectra (Fig. 8) it is seen that scattering loss in the lower wavelength side is more than in the higher wavelength side. Therefore, lower the wavelength of light higher the scattering loss and vice versa. From XRD the particle diameter and from FESEM the number density and volume of the particles is found to be increased with heat-treatment time. Hence the scattering loss is supported by the Eq. (2), where the refractive index of the formed crystal phase is more than the residual glass phase.

3.7 Emission, excitation and lifetime

Figs. 9(a) and 9(b) depict the visible and infrared emission spectra respectively of as-prepared precursor glass and samples heat-treated for 2, 50 and 100 h durations. The excitation spectra of these four samples measured in the wavelength range 600–1000 nm by monitoring with the intense NIR emission located at 1540 nm as shown in Fig. 10. In Fig. 9(a), the spectrum of the as-prepared glass sample emits bright green light under 377 nm ($^4I_{15/2} \rightarrow {}^4G_{11/2}$) excitation. The 515-542 and 542-577 nm green bands correspond to the $^2H_{11/2} \rightarrow {}^4I_{15/2}$ and $^4S_{3/2} \rightarrow {}^4I_{15/2}$ transitions respectively. The former band was resolved with Stark splitting at 527 and 535 nm, and the latter revealed the same with peaks at 550 and 559 nm respectively. The heat-treated samples exhibited the same emission profile as the precursor glass. But the emission band $^2H_{11/2} \rightarrow {}^4I_{15/2}$ freezes out at the initial stages of heat-treatment and the intensity increases with increase in heat-treatment time. This may be due to the very rapid thermal phonon relaxation from the $^2H_{11/2}$ level to the $^4S_{3/2}$ level [36]. The directly excited 980 nm emission spectra of the as prepared glass and the heat-treated samples exhibits emission from $^4I_{13/2}$ excited level to the $^4I_{15/2}$ ground level with Stark splitting at 1537 and 1566 nm. With increase in heat-treatment time the peak at 1537 nm for glass shifted to 1540 nm for 100 h heat-treated sample. In the case of precursor glass the full width at half maximum (FWHM) of the peak at 1550 nm is ~78 nm which is less than that of antimony-borosilicate glasses (FWHM = 90 nm) [37] but equivalent to tellurite glasses (FWHM = 77 nm) [38]. The FWHM further decreases down to ~56 nm for the heat-treated samples. Similarly, the peak intensity ratio at 1566 nm to 1540 nm for precursor glass is ~0.93 which decreases down to ~0.79 for the heat-treated samples. It is generally seen that the glass-ceramics

samples show more intense photoluminescence than the as-prepared glass. In our case it is found that the fluorescence intensity first decreases for the glass-ceramics heat-treated for shortest duration (2h) and then increases but with low intense than as-prepared glass. The reason behind this may be the fact that in the short durations of heat-treatment the samples are phase separated and stable $KNbO_3$ phase grows with longer heat-treatment duration. This is also supported by the dielectric data as described earlier. The shifting in the peak positions in emission spectra of glass-ceramics and the decrease of the FWHM value could establish the fact that the rare earth ions enter but in a less amount into the crystalline phase thus formed. In fact, we have generated nanocrystal of $KNbO_3$ in Er^{3+}-doped K_2O-Nb_2O_5-SiO_2 glasses. Consequently, it results in initial formation of $KNbO_3$ nanocrystals followed by incorporation of Er^{3+} into the $KNbO_3$ crystals, and further growth and formation of more $KNbO_3$ crystals. These facts could clearly be understood if we analyze the UV-vis and NIR emission spectral profiles and evolution as shown in Fig. 9. Kang, *et. al* [39] have also observed a similar less intense fluorescence in glass-ceramics than the as prepared glass of neodymium activated lithium alumino silicate system. These results are in similar trend when we used Eu^{3+} as the doping ion in this K_2O-Nb_2O_5-SiO_2 glass [34]. In that system we reported photoluminescence emission in the visible region (500-725 nm). But in this present system we are reporting photoluminescence emission in the visible (450-650 nm) and NIR region (1450-1650 nm) of Er^{3+}. The Eu^{3+} and Er^{3+} ions have different energy levels and different types of applications. For example, Eu^{3+} ion exhibit red emission around 600 nm whereas the Er^{3+} ion exhibit green emission around 550 nm and 1550 nm NIR emission. Moreover, in the NIR region, exciting at 1550 nm second harmonic generation at 775 nm could be

possible. For these reasons in the present study we are investigating the case of Er^{3+} as the doping ion. As mentioned earlier, the photoluminescent intensity of Er^{3+} ion is strongly dependent on the surrounding chemical environment. For strong luminescent intensity, the said ion must be incorporated in a non-centrosymmetric host. Generally, in the perovskite type $RNbO_3$ (R = Li, Na, K) crystals, R^+ and Nb^{5+} occupy octahedral sites with C_3 or nearly C_{3v} point symmetry. When the rare earth ion is entering in the crystal, it prefers to replace R^+ site forming $[REO_6]^{9-}$ octahedron [40-42]. Here also, the Er^{3+} ions replace K^+ ion sites in the formed $KNbO_3$ crystallites due to the closeness of their ionic radii (Er^{3+} = 0.89 Å and K^+ = 1.38 Å). However, still there exists slight difference in the ionic radius between the dopant (Er^{3+}) and the host ions (K^+) along with the excess electronic charge on the dopant. Generally, when the impurity ion carries extra charge than the replaced host ion, the electrostatic force acting on the impurity is greater than that on the host ion, the impurity ion will pull the oxygen ligands inwards along RE–ligand bonds, creating distortion in the lattice structure and as a result, distorted $[ErO_6]^{9-}$ octrahedron is formed with Er^{3+} ion facing an off-center displacement from C_3 axis in the oxygen octahedron [43]. Also the decrease in the peak intensity ratio at 1566 nm to 1540 nm for the heat-treated samples furnishes that Er^{3+} ions are in a distorted manner in the formed $KNbO_3$ phase. The above results are in conformity with XRD, FESEM, TEM and FTIRRS results.

Fig. 11 presents representative curves of the room temperature fluorescence decay of the emission transition ($^4I_{13/2} \rightarrow {}^4I_{15/2}$) at 1540 nm with an excitation at 980 nm for Er^{3+} ions in as-prepared glass and heat-treated samples for 2 and 50 h. All the curves demonstrate a single exponential decay. The fluorescence lifetimes (τ_f) for all the samples

have been estimated from these decay curves and the results of 0, 2 and 50 h duration are shown in Table 2. These data indicate a decrease in the lifetime at the start of the heat-treatment and then an increasing trend with an increase in the heat-treatment duration following the similar trend as the emission characteristics. It is clear that the excited state lifetime of Er^{3+} ions initially has decreased from 2656 µs for precursor glass down to 2316 µs for 2 h heat-treated sample and then noticeably increases up to 4519 µs for 50 h heat-treatment. The decrease in the lifetime first and then subsequent increase for further increase in heat-treatment duration may be attributed to the possible occurrence of surface defects and/or clustering of Er^{3+} ions in the initial stage which act as luminescence quenchers. This may also be the reason for the observed reduction in the luminescence intensity of heat-treated glass-ceramics when compared to the as-prepared glass (see Fig. 9(a), 9(b)). Dejneka [35] have demonstrated in fluoride glasses that clustering thereby quenching occur when the Eu^{3+}-Eu^{3+} ionic separation is less than 40 Å. In the present case, the Er^{3+}-Er^{3+} ionic separation (R_i) in the precursor glass is found to be about 26 Å which was calculated using the relation [44]:

$$R_i \text{ (Å)} = (1/N_{Er}^{3+})^{1/3} \qquad\qquad (3)$$

where N_{Er}^{3+} is the Er^{3+} ion concentration which is already provided in Table 1. It is, therefore, seen that the Er^{3+}-Er^{3+} ionic separation (R_i) is in the quenching region. Theoretically, the rate of relaxation due to concentration quenching varies as R_i^{-6} [44, 45]. In the initial stages of heat-treatment with the formation of $KNbO_3$ crystal phase, the Er^{3+} ions partitioned into the residual glassy phase by reducing the inter-ionic separation less than 26 Å of precursor glasses. This fact results in reduction in fluorescence intensity (see curve for 2 h, Fig. 9) due to concentration quenching. Later with the increase of heat-

treatment time, the Er^{3+} ions become well organized and finely dispersed in the crystal phase, thereby increasing the intensity of fluorescence. Subsequent increase in lifetime is due to partitioning of Er^{3+} ions into low phonon energy (~749 cm^{-1}) $KNbO_3$ crystal from high phonon energy (~1128 cm^{-1}) mother silicate glass matrix. This process results in reduction in nonradiative decay rate due to multiphonon relaxation thereby rising in radiative decay rate. Thus, the measured fluorescence lifetime (τ_f) may be well explained by the following expression [16]:

$$\tau_f = 1/(A_{rad} + W_{nr}) \tag{4}$$

where A_{rad} and W_{nr} are the probabilities for radiative and nonradiative processes respectively. The W_{nr} includes relaxation by multiphonon emission and effective energy transfer rates arising from Er^{3+}-Er^{3+} ion interactions, that is, cross relaxation (CR) and energy migration (EM).

4. Conclusions

Er_2O_3 (0.5 wt %) doped $KNbO_3$ nanocrystallites containing glass-ceramics were prepared from the glass $25K_2O$-$25Nb_2O_5$-$50SiO_2$ (mol %) by an isothermal crystallization at 800^oC for different durations. The formation of nano-crystallite of $KNbO_3$ in the glass matrix was confirmed by the XRD, FESEM, TEM, FTIRRS and dielectric constant measurements. The crystallite size estimated from XRD and TEM is found to vary in the range of 7-15 and 14-23 nm respectively. The optical absorption spectra, decay time fluorescence spectra of heat-treated glass-ceramic samples demonstrate that the Er^{3+} ion has gradually entered into the $KNbO_3$ crystalline phase.

Acknowledgements

References

[1] M. Zgonik, R. Schlesser, I. Biaggio, E. Voit, J. Tscherry, P. Giinter, J. Appl. Phys. 74 (1993) 1287-1297.

[2] D. F. Xue, S. Y. Zhang, Chem. Phys. Lett. 291 (1998) 401-406.

[3] W. P. Risk, T. R. Gosnell, A. V. Nurmikko, Compact Blue-Green Lasers, Cambridge University Press, Cambridge, 2003, p. 21.

[4] E. Ringgaard, T. Wurlitzer, J. Eur. Ceram. Soc. 25 (2005) 2701-2706.

[5] D. E. Vernacotola, Key Engg. Mater. 94-95 (1994) 379-408.

[6] P. Pernice, A. Aronne, V. N. Sigaev, P. D. Sarkisov, V. I. Molev, S. Y. Stefanovich, J. Am. Ceram. Soc. 82 (1999) 3447-3452.

[7] P. Pernice, A. Aronne, V. N. Sigaev, M. Kupriyanova, J. Non-Cryst. Solids 275 (2000) 216-224.

[8] V. V. Golubkov, O. S. Dymshits, A. A. Zhilin, A. V. Redin, M. P. Shepilov, Glass Phys. Chem. 27 (2001) 504-511.

[9] H. Tanaka, M. Yamamoto, Y. Takahashi, Y. Benino, T. Fujiwara, T. Komatsu, Opt. Mater. 22 (2003) 71-79.

[10] A. Aronne, V. N. Sigaev, P. Pernice, E. Fanelli, L. Z. Usmanova, J. Non-Cryst. Solids 337 (2004) 121-129.

[11] S. Dai, J. Wu, J. Zhang, G. Wang, Z. Jiang, Spectrochim. Acta A, 62 (2005) 431-437.

[12] D. C. Winburn, Practical Laser Safety, New York, Dekker, 1985.

[13] Y. Y. Hui, P-H. Shih, K-J. Sun, C-F. Lin, Thin Solid Films, 515 (2007) 6754-6757.

[14] A. Z. Simões, A. Ries, C. S. Riccardi, A. H. Gonzalez, M. A. Zaghete, B. D. Stojanovic, M. Cilense, J. A. Varela, Mat. Lett. 58 (2004) 2537-2540.

[15] M. B. Volf, Chemical Approach to Glass, Elsevier, Amsterdam-Oxford-New York-Tokyo, 1984.

[16] M. Yamane, Y. Asahara, Glasses for Photonics, Cambridge University Press, Cambridge, UK, (2000).

[17] D. E. Vernacotola, J. E. Shelby, Phys. Chem. Glasses 35 (1994) 153-159.

[18] D. E. Vernacotola, J. E. Shelby, Ceram. Trans. 29 (1993) 215-220.

[19] E. D. Palik, Handbook of Optical Constants of Solids III, Academic Press, San Diego, 1998, p. 834.

[20] B. D. Cullity, Elements of X-Ray Diffraction, 2nd ed. Addison-Wesley Publishing Co., London, U. K., 1977.

[21] A. Aronne, V. N. Sigaev, B. Champagnon, E. Fanelli, V. Califano, L. Z. Usmanova, P. Pernice, J. Non-Cryst. Solids 351 (2005) 3610-3618.

[22] S. Bhattacharyya, Th. H□che, N. Hemono, M. J. Pascual, P. A. van Aken, J. Cryst. Growth 311 (2009) 4350-4355.

[23] K. Fukumi, S. Sakka, J. Mater. Sci., 23 (1988) 2819-2823.

[24] B. Sumuneva, St. Kralchev, V. Dimitrov, J. Non-Crys. Solids, 129 (1991) 54-63.

[25] J. S. deAndrade, A. G. Pinheiro, I. F. Vasconcelos, M. A. B. deArujo, M. A. Valente, A. S. B. Sombra, J. Phys. Chem. Solids 61 (2000) 899-906.

[26] E. N. Silva, A. P. Ayala, I. Guedes, C. W. A. Paschoal, R. L. Moreira, C. K. Loong, L. A. Boatner, Opt. Mater. 29 (2006) 224-230.

[27] D. Mandal, H. D. Banerjee, M. L. N. Goswami, H. N. Acharya, Bull. Mater. Sci., 27

(2004) 367-372.

[28] S. N. B. Bhaktha, B. Boulard, S. Chaussedent, A. Chiappini, A. Chiasera, E. Duval, C. Duverger, S. Etienne, M. Ferrari, Y. Jestin, M. Mattarelli, M. Montagna, A. Monteil, E. Moser, H. Portales, K. C. Vishunubhatla, Opt. Mater, 28 (2006) 1325-1328.

[29] Q. Qian, Y. Wang, Q. Y. Zhang, G. F. Yang, Z. M. Yang, Z. H. Jiang, J. Non. Cryst. Solids, 354 (2008) 1981-1985.

[30] A. Nayak, P. Kundu, R. Debnath, J. Non. Cryst. Solids, 353 (2007) 1414-1417.

[31] H. Lin, K. Liu, E. Y. B. Pun, T. C. Ma, X. Peng, Q. D. An, J. Y. Yu, S. B. Jiang, Chem. Phys. Lett. 398 (2004) 146-150.

[32] T. Schweizer, D. J. Brady, D. W. Hewak, Opt. Exp. 1 (1997) 102-107.

[33] W. T. Carnall, P. R. Fields, K. Rajnak, J. Chem. Phys. 49 (1968) 4424-4442.

[34] R. S. Chaliha, K. Annapurna, A. Tarafder, V. S. Tiwari, P. K. Gupta, B. Karmakar, Solid State Sci. 11 (2009) 1325–1332.

[35] M. J. Dejneka, J. Non-Cryst. Solids 239 (1998) 149-155.

[36] S. A. Klimin, E. P. Chukalina, M. N. Popova, E. Antic-Fidancev, P. Aschehoug, N. V. Gaponenko, I. S. Molchan, D. A. Tsyrkunov, Phy. Lett. A 323 (2004) 159-163.

[37] Q. Qian, C. Zhao, G. F. Yang, Z. M. Yang, Q. Y. Zhang, Z. H. Jiang, Spectrochim. Acta A, 71 (2008) 280-285.

[38] Y. Gao, Q-H. Nie, T-F. Xu, X. Shen, Spectrochim. Acta A, 61 (2005) 1259-1262.

[39] UK Kang, A. A. Zhilin, D. P. Logvinov, A. A. Onushchenko, V. A. Savost'yanov, T. I. Chuvaeva, A.V. Shashkin, Glass Phys. Chem. 27 (2001) 344-352.

[40] S. Y. Wu, W. C. Zheng, Phys. Rev. B 65 (2002) 224107-224112.

[41] S. Y. Wu, H. N. Dong, J. Alloy. Comp. 386 (2005) 52-56.

[42] Y. M. Chang, T. H. Yeom, Y. Y. Yeung, C. Rudowicz, J. Phys.: Conds. Mater. 5 (1993) 6221-6230.

[43] D. M. B. P. Milori, I. J. Moraes, A. C. Hernandes, R. R. de Souza, M. Siu Li, M. C. Terrile, G. E. Barberis, Phys. Rev. B 51 (1995) 3206-3209.

[44] K. Pátek, Glass Lasers, Butterworth & Co (Publishers) Ltd., London, 1970.

[45] J. H. Campbell, T. I. Suratwala, J. Non-Cryst. Solids 263 & 264 (2000) 318-341.

Figure Captions

Fig. 1. DTA curve of as-prepared precursor glass powder.

Fig. 2. (Color online) Photograph showing the transparency, as laid on writing, of the (a) as-prepared glass and heat-treated samples at 800°C for (b) 1, (c) 2, (d) 3, (e) 5, (f) 10, (g) 25, (h) 50 and (i) 100 h.

Fig. 3. Variation of refractive indices of precursor glass and glass-ceramics obtained after heat-treatment for different duration as a function of wavelength.

Fig. 4. (a) XRD patterns of as-prepared glass and heat-treated glasses at 800°C for different duration. (b) Variation of crystallite size, as obtained from XRD, as a function of heat-treatment time at 800°C of as-prepared glasses.

Fig. 5. FESEM photomicrograph of heat-treated glasses at 800°C for (a) 3 and (b) 50 h (scale bar = 100 nm). TEM image of 50 h heat-treated sample (c) bright field image (inset: SAED), and (d) HRTEM image of lattice fringe.

Fig. 6. Comparative FTIRR spectra of the precursor glass and heat-treated glasses at 800°C for 2 and 100 h. Inset shows the reflectivity at 930 and 749 cm^{-1} of precursor glass and heat-treated glasses as a function of heat-treatment time.

Fig. 7. Dielectric constant of as-prepared glass and glass-ceramics as a function of heat-treatment time at 800°C.

Fig. 8. Absorption spectra of the as-prepared glass and heat-treated glasses at 800°C for 2, 50 and 100 h (a. u. = absorbance unit).

Fig. 9. (a) Visible emission spectra (λ_{ex} = 377 nm) and (b) near infrared emission spectra (λ_{ex} = 980 nm) of the as-prepared glass and heat-treated glasses at 800°C for 2, 50 and 100 h (a. u. = arbitrary unit).

Fig. 10. Excitation spectra (λ_{em} = 1540 nm) of the as-prepared glass and heat-treated glasses at 800°C for 2, 50 and 100 h (a. u. = arbitrary unit).

Fig. 11. (Color online) Decay curves for the $^4I_{13/2} \rightarrow {}^4I_{15/2}$ transition at 1540 nm under excitation at 980 nm of as-prepared glass and heat-treated glasses at 800°C for 2 and 50 h (a. u. = arbitrary unit).

Table 1
Some measured and calculated properties of $25K_2O-25Nb_2O_5-50SiO_2$
(mol %) glass with 0.5 wt% Er_2O_3 (in excess)

Properties	Corresponding value
Average molecular weight	120.05
Density, $g.cm^{-3}$	3.37
Refractive index	
n_e (at 546.1 nm)	1.78076
$n_F{'}$ (at 480.0 nm)	1.79612
$n_C{'}$ (at 643.8 nm)	1.76688
Mean dispersion ($n_F{'} - n_C{'}$)	0.02924
Abbe number, $n_e/(n_F{'}-n_C{'})$	27
Reflection loss (%)	7.88
Molar refractivity, R_M (cm^3)	14.95
Electronic polarizability, α (cm^3)	5.592×10^{-24}
Er^{3+} ion concentration, $N_{Er}{}^{3+}$ (ions/cm^3)	5.41×10^{19}
Er^{3+}-Er^{3+} inter ionic distance, R_i (Å)	26
Glass transition temperature, T_g (^oC)	681
Crystallization peak, T_p (^oC)	759

Table 2
Relative intensity ratio of I_{Nb-O}/I_{Si-O} from FTIRR
spectra and measured lifetime (τ_f) of the
$^4I_{13/2} \rightarrow {}^4I_{15/2}$ emission transition of precursor
and heat treated (at 800^oC) Er^{3+} doped glasses

Samples	Relative intensity ratio, I_{Nb-O} / I_{Si-O}	Lifetime, τ_f (µs)
Glass	-	2656
2h	1.06	2316
50h	1.12	4519
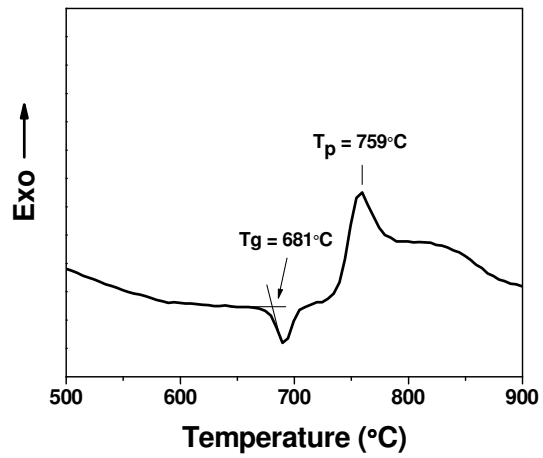
Fig. 1. DTA curve of as-prepared precursor glass powder.
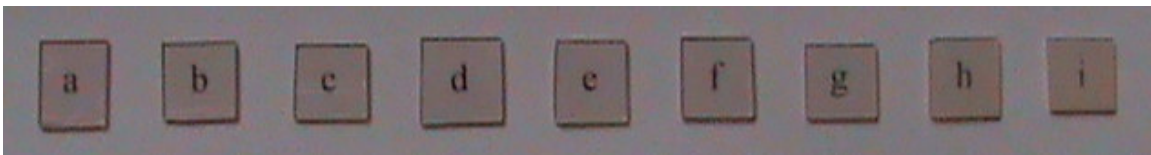
Fig. 2. (Color online) Photograph showing the transparency, as laid on writing, of the (a) as-prepared glass and heat-treated samples at 800°C for (b) 1, (c) 2, (d) 3, (e) 5, (f) 10, (g) 25, (h) 50 and (i) 100 h.
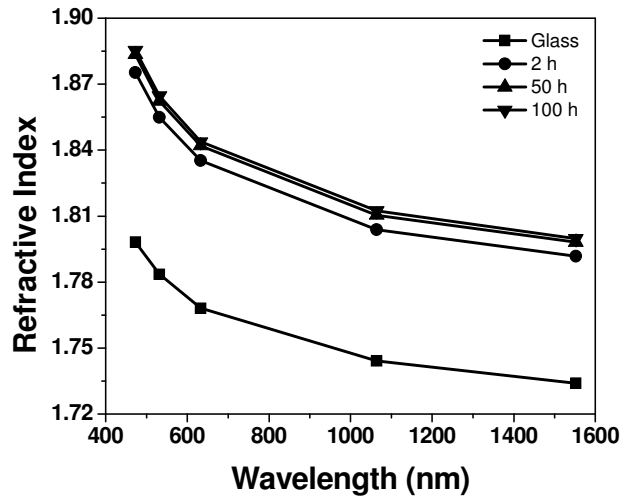
Fig. 3. Variation of refractive indices of precursor glass and glass-ceramics obtained after heat-treatment for different duration as a function of wavelength.
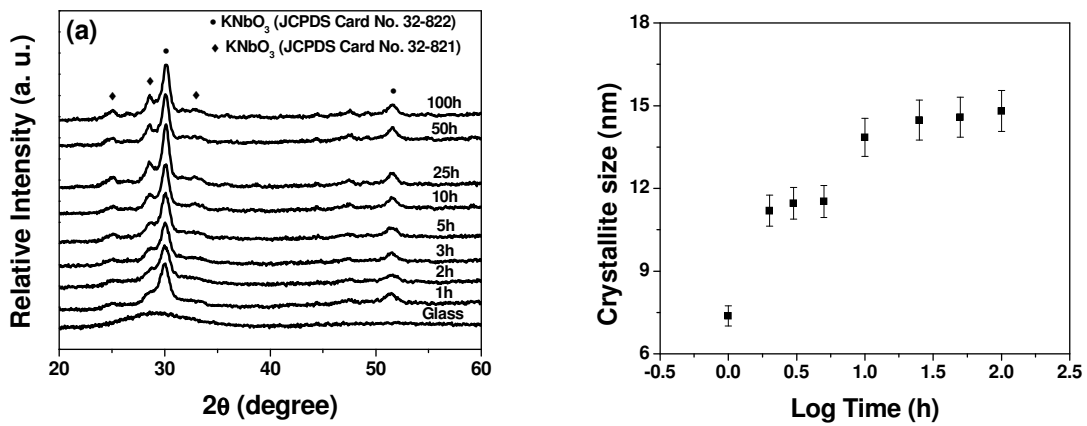

Fig. 4. (a) XRD patterns of as-prepared glass and heat-treated glasses at 800°C for different duration. (b) Variation of crystallite size, as obtained from XRD, as a function of heat-treatment time at 800°C of as-prepared glasses.
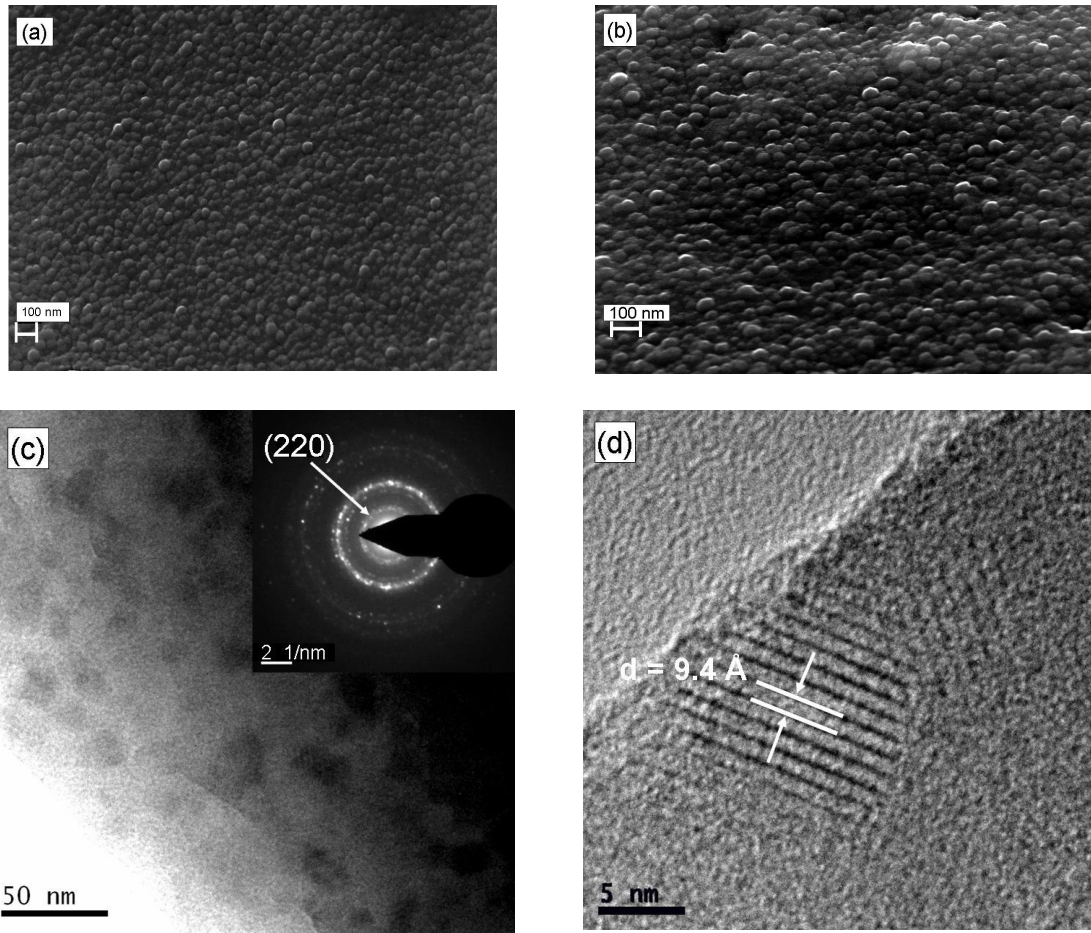
Fig. 5. FESEM photomicrograph of heat-treated glasses at 800°C for (a) 3 and (b) 50 h (scale bar = 100 nm). TEM image of 50 h heat-treated sample (c) bright field image (inset: SAED), and (d) HRTEM image of lattice fringe.
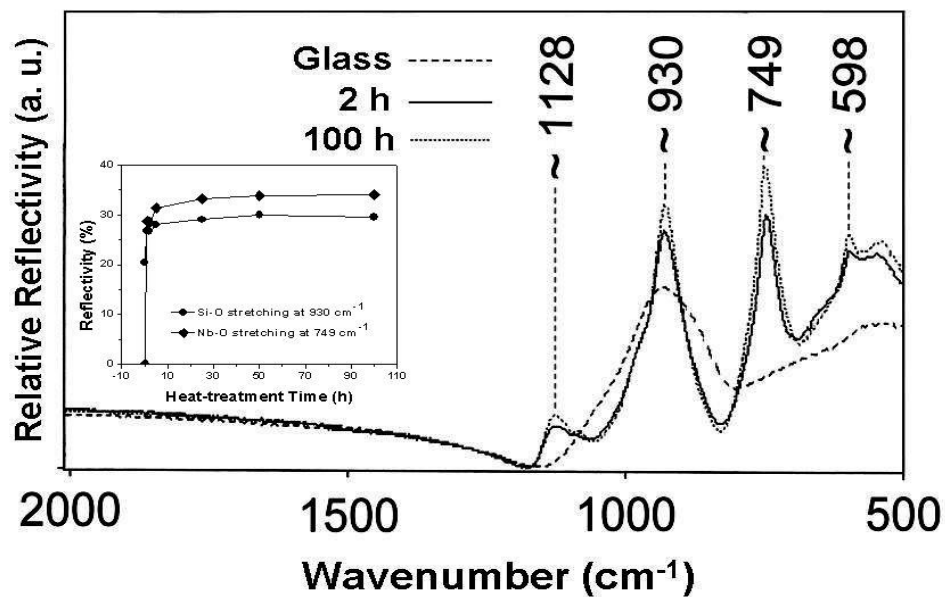
Fig. 6. Comparative FTIRR spectra of the precursor glass and heat-treated glasses at 800°C for 2 and 100 h. Inset shows the reflectivity at 930 and 749 cm^{-1} of precursor glass and heat-treated glasses as a function of heat-treatment time.
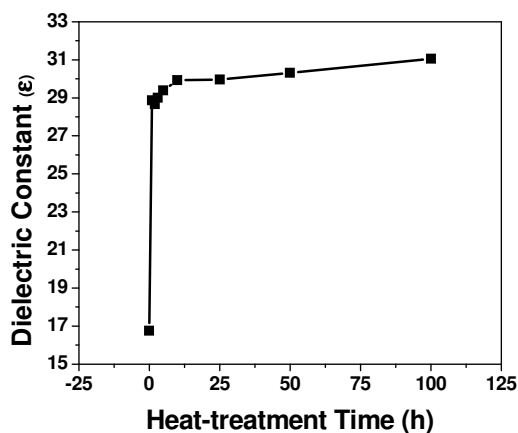

Fig. 7. Dielectric constant of as-prepared glass and glass-ceramics as a function of heat-treatment time at 800°C.

Fig. 8. Absorption spectra of the as-prepared glass and heat-treated glasses at 800°C for 2, 50 and 100 h (a. u. = absorbance unit).
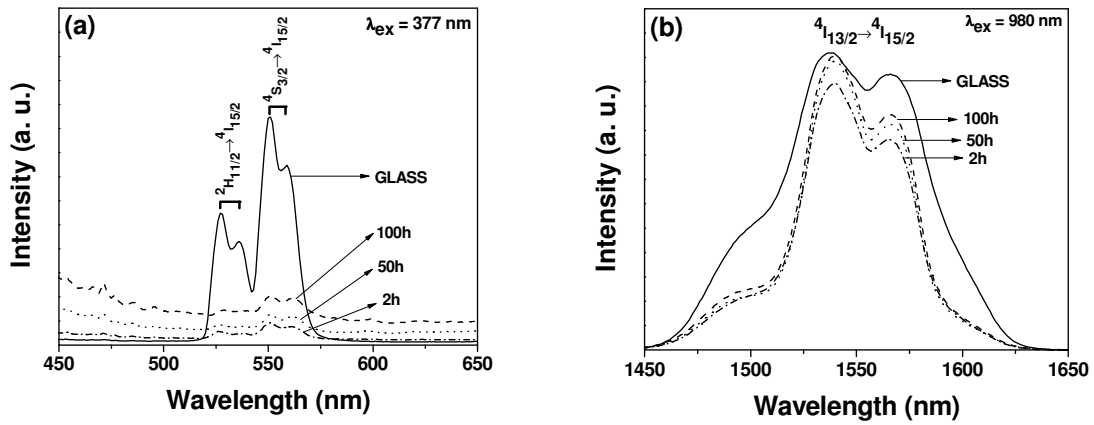

Fig. 9. (a) Visible emission spectra (λ_{ex} = 377 nm) and (b) near infrared emission spectra (λ_{ex} = 980 nm) of the as-prepared glass and heat-treated glasses at 800°C for 2, 50 and 100 h (a. u. = arbitrary unit).
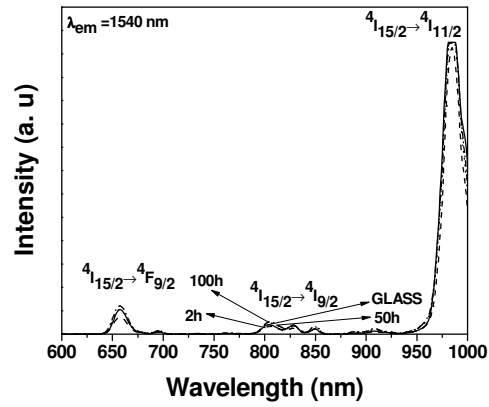
Fig. 10. Excitation spectra (λ_{em} = 1540 nm) of the as-prepared glass and heat-treated glasses at 800°C for 2, 50 and 100 h (a. u. = arbitrary unit).
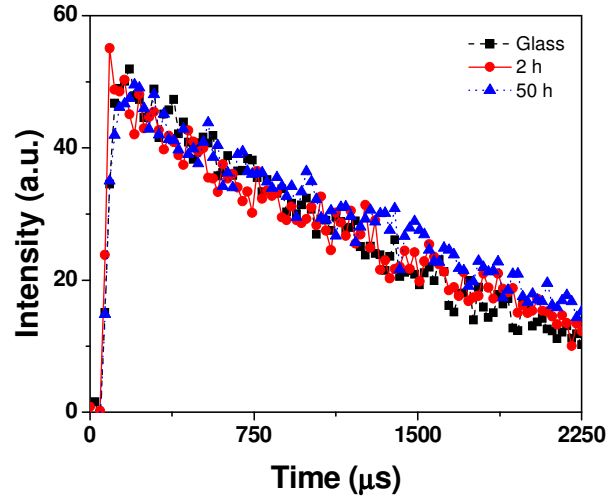

Fig. 11. (Color online) Decay curves for the $^{4}I_{13/2} \to {}^{4}I_{15/2}$ transition at 1540 nm under excitation at 980 nm of as-prepared glass and heat-treated glasses at 800°C for 2 and 50 h (a. u. = arbitrary unit).